International Journal of Heat and Mass Transfer 53 (2010) 2035–2043

Contents lists available at ScienceDirect

International Journal of Heat and Mass Transfer

journal homepage: www.elsevier.com/locate/ijhmt

Investigation of steel emissivity behaviors: Examination of Multispectral Radiation Thermometry (MRT) emissivity models

Chang-Da Wen *

Department of Mechanical Engineering, National Cheng Kung University, No. 1, University Road, Tainan 701, Taiwan

ARTICLE INFO

Article history:
Received 29 June 2009
Received in revised form 3 December 2009
Accepted 3 December 2009
Available online 1 February 2010

Keywords:
Steel
Emissivity
Temperature measurement
Multispectral Radiation Thermometry

ABSTRACT

Steel emissivity behaviors were investigated in this study. Experiments were conducted to measure emissivity. Six emissivity models were then applied to examine Multispectral Radiation Thermometry (MRT) on inferring surface temperature. The data show that emissivity decreases with increasing wavelength. For steel containing high chromium, emissivity is usually lower than others because of the chromium oxide protection layer. Two emissivity models provide the best overall compensation for different alloys, number of wavelengths, and temperatures. The results reveal that if the emissivity model can well represent the real emissivity behaviors, the more accurate inferred temperature can be achieved.

1. Introduction

Steel is the most important metal in the world due to its undeniable features, such as strength, hardness, ease of fabrication, fire and heat resistance, impact resistance, and corrosion resistance. It has been used extensively in many applications, from small metallic parts and tools to large structural members of architecture and aircraft.

With increasing industry competitiveness, the requirements for higher product quality and cost consciousness have forced the steel industry to develop more efficient and effective techniques to produce better products and less waste. One of the most critical issues about how to achieve higher performance in manufacturing process is to accurately measure the metal surface temperature.

Many processes in steel manufacturing, such as forging, extrusion, and rolling are required to accurately measure the surface temperature in order to obtain metallurgical quality, to improve product reliability and reproducibility, and to reduce production cost.

At present, the thermocouple or other types of contact thermometers are very commonly used to measure the surface temperature in industry. However, in some processes, contact temperature measurement methods are undesirable because the contact may not be feasible in moving material situations and may change the surface physically or chemically. Additionally, the contact method currently in use may not be accurate enough to meet the industry requirement. As a result, a need exists for a more accurate, nondestructive and more simple approach. One such approach is a non-contact radiometric method.

Radiation thermometry, a convenient, non-contact temperature measurement method, utilizes the intensity of thermal radiation measured from the target surface to infer the true temperature. The foundation of this concept states that using fundamental electromagnetic wave theory, the measured intensity is used to infer the temperature of the surface when referenced to an ideal surface called a *blackbody*. The spectral intensity emitted by a blackbody at temperature T can be obtained by the Planck distribution

$$L_{\lambda,b}(\lambda,T)=\frac{c_1}{\lambda^5\left(e^{\frac{c_2}{\lambda T}}-1\right)}, \tag{1}$$

where, $c_1 = 1.19\times10^8$ W μm^4 m^{-2} sr^{-1} and $c_2 = 1.439\times10^4$ μm K. Since the blackbody is an ideal emitter, the intensity of radiation emitted from a real surface will be smaller than from a blackbody at the same temperature. *Emissivity*, a surface radiative property is defined as the ratio of intensity of radiation emitted by a surface to that emitted by a blackbody at the same temperature. Therefore, spectral emissivity can be expressed as

$$\varepsilon_\lambda(\lambda,T)=\frac{L_{\lambda,e}(\lambda,T)}{L_{\lambda,b}(\lambda,T)}. \tag{2}$$

The spectral intensity, $L_{\lambda,meas}$, measured by the radiation thermometer can be consisted of four components,

$$L_{\lambda,meas}(\lambda,T)=L_{\lambda,e}(\lambda,T)+L_{\lambda,ref}+L_e+L_s, \tag{3}$$

where $L_{\lambda,e}$ is the self-emitted intensity from the target, $L_{\lambda,ref}$ is the intensity from the surrounding irradiation reflected by the target

* Tel.: +886 6 2757575x62110; fax: +886 6 2352973.
E-mail address: alexwen@mail.ncku.edu.tw

0017-9310/$ - see front matter © 2009 Elsevier Ltd. All rights reserved.
doi:10.1016/j.ijheatmasstransfer.2009.12.053

Nomenclature

a_0	first unknown coefficient of emissivity model
a_1	second unknown coefficient of emissivity model
c_1	first thermal radiation constant
c_2	second thermal radiation constant
DWRT	dual-wavelength radiation thermometry
HRR	Hagen–Rubens Relation emissivity model
IST	inverse spectral temperature emissivity model
IWS	inverse wavelength squared emissivity model
L_e	spectral intensity of target surface emission reflected back by surroundings
L_s	spectral intensity of radiation associated with scattering and absorption
$L_{\lambda,b}$	spectral intensity of blackbody radiation
$L_{\lambda,e}$	spectral intensity of radiation emitted by target surface
$L_{\lambda,gen}$	generated spectral intensity of radiation
$L_{\lambda,meas}$	measured spectral radiation intensity
$L_{\lambda,ref}$	spectral intensity of irradiation from surroundings that is reflected by target surface
MRT	Multispectral Radiation Thermometry
m	number of unknown coefficients of emissivity model
n	required minimum number of wavelengths
N	total number of wavelength available in the examined wavelength range
SRT	spectral radiation thermometry
T	surface temperature
T_P	predicted temperature by radiation thermometry
T_{sur}	temperature of surroundings
T_λ	spectral radiance temperature
T.E.	temperature error
WLT	wavelength temperature emissivity model

Greek symbols

ε_λ	spectral emissivity
λ	wavelength
ρ_λ	spectral reflectivity
χ^2	least-squares error

Subscripts

b	blackbody
e	emitted
gen	generated
$meas$	measured
p	predicted
ref	reflected
s	scatted
sur	surroundings
λ	spectral

surface, L_e is due to the target irradiation reflected by the surrounding and then target itself, and L_s is from the atmospheric scattering and absorption (H_2O, CO_2, dust particles, etc.). If the radiation exchange between the target and surrounding is between a small and a large enclosure, the term L_e can be neglected due to the blackbody assumption of the surrounding. In the absence of atmospheric line-of-sight absorption or emission, then the term L_s is also negligible. Therefore, the measured intensity of an opaque target surface, $L_{\lambda,meas}$, can be simplified as

$$L_{\lambda,meas}(\lambda,T) \cong L_{\lambda,e}(\lambda,T) + L_{\lambda,ref} = \varepsilon_\lambda L_{\lambda,b}(\lambda,T) + \rho_\lambda L_{\lambda,b}(\lambda,T_{sur}), \tag{4}$$

where ρ_λ is the spectral reflectivity of the target surface defined as the fraction of the intensity of irradiation from the surroundings (at T_{sur}) that is reflected by the target surface. From the law of energy conservation and the application of Kirchhoff's law, for an opaque material the reflectivity can be determined as

$$\rho_\lambda = 1 - \varepsilon_\lambda. \tag{5}$$

Therefore, inserting Eq. (5) into (4) yields the following popular expression for the measured radiation intensity of an opaque target surface,

$$L_{\lambda,meas}(\lambda,T) = \varepsilon_\lambda L_{\lambda,b}(\lambda,T) + (1-\varepsilon_\lambda) L_{\lambda,b}(\lambda,T_{sur}), \tag{6}$$

where both $L_{\lambda,b}(\lambda,T)$ and $L_{\lambda,b}(\lambda,T_{sur})$ can be calculated from the Planck distribution, Eq. (1). With known ε_λ, the target surface temperature T can be determined by the Eq. (6) from the measured spectral intensity, $L_{\lambda,meas}$. If the temperature of a target surface is much hotter than the environmental temperature, which means $L_{\lambda,b}(\lambda,T) >> L_{\lambda,b}(\lambda,T_{sur})$, then the second term on the right-hand-side of Eq. (6) can be neglected without compromising measurement accuracy. However, this may not always be suitable in steel production environment.Determining temperature can be accomplished by three categories of radiation thermometry, which utilize intensity measurements at a differing number of wavelengths: these three types are spectral, dual-wavelength and multispectral. Spectral radiation thermometry (SRT) requires the intensity measurement at one wavelength and a constant emissivity value to infer the surface temperature. Dual-wavelength radiation thermometry (DWRT) employs the intensity measurements at two distinct wavelengths and an emissivity compensation algorithm to determine the surface temperature. Multispectral Radiation Thermometry (MRT) utilizes the intensity measurements at three or more discrete wavelengths and an emissivity model to obtain the surface temperature. The MRT method is preferred for its ability to enhance measurement accuracy as well as account for the complex spectral variations of both radiation intensity and emissivity.

2. Multispectral Radiation Thermometry (MRT)

Multispectral Radiation Thermometry, an extension of the dual-wavelength methods, observes the spectral radiance at three or more wavelengths and deduces the real surface temperature by assuming a general model of the emissivity behavior. Either (1) empirical functions based upon measured spectral emissivity values or (2) analytical functions developed from theoretical model premises describe the emissivity model. Six MRT emissivity models are examined in this study for accuracy in temperature determination: Hagen–Rubens Relation (HRR) model [1–7], inverse spectral temperature (IST) model [4–7], inverse wavelength squared (IWS) model [5–8], and wavelength temperature (WLT) model [4,6,7,9], and two variations to IST and WLT models (IST* and WLT*).

$$\text{HRR}: \varepsilon_\lambda = a_0 \times \left(\frac{T_P}{\lambda}\right)^{1/2}, \tag{7}$$

$$\text{IST}: \varepsilon_\lambda = \exp\left(\frac{a_0}{T_\lambda}\right), \tag{8}$$

$$\text{IWS}: \varepsilon_\lambda = \frac{1}{1 + a_0 \lambda^2}, \tag{9}$$

$$\text{WLT}: \varepsilon_\lambda = \exp(a_0\lambda + a_1 T_P), \tag{10}$$

$$\mathrm{IST}^{*}: \varepsilon_\lambda = \exp\left(a_0 + \frac{a_1}{T_\lambda}\right), \tag{11}$$

$$\mathrm{WLT}^{*}: \varepsilon_\lambda = \exp\left(a_0\lambda + \frac{a_1}{T_\lambda}\right), \tag{12}$$

where, a_0, a_1 are the unknown coefficients in the emissivity model, T_P is the predicted temperature, and T_λ in models IST, IST*, and WLT*, is the spectral radiance temperature which is the equivalent blackbody temperature of the measured spectral intensity.

The unfixed coefficient values in the emissivity model allow the multispectral radiation methods to have enough selectivity to represent the variable emissivity behaviors and are less affected by noise. Moreover, the increased number of wavelengths also allow for the statistical reduction in temperature errors from measurement noise.

Two different mathematical techniques of Multispectral Radiation Thermometry are used to infer the temperature. The first method is the *exact technique* which employs radiation intensity measurements at $m+1$ wavelengths when using an emissivity model with m unknown coefficients. This results in $m+1$ equations with $m+1$ unknowns: the target surface temperature, T, and the m unknown coefficients in the emissivity model while applying Eq. (6). Coates [10] and Doloresco [11] concluded that the exact technique might cause *over-fitting* and result in large errors when using more than three wavelengths. The other method which can overcome the over-fitting problem is the *least-squares* technique. It employs least-squares fitting of the measured radiances to simultaneously deduce the best-fit values of emissivity and temperature. This technique is commonly used in MRT and has been studied by numerous researchers. The m unknown coefficients in the emissivity model must be at least two fewer than the number of the spectral radiance values for the least-squares technique, i.e., spectral intensity measurements at a minimum of $(m+2)$ wavelengths.

The rationale is to determine the inferred temperature and the unknown emissivity coefficients by minimizing the chi-squared (χ^2) value of the following equation

$$\chi^2 = \sum_{i=0}^{n} (L_{\lambda,meas,i} - L_{\lambda,gen,i})^2, \tag{13}$$

where $L_{\lambda,meas,i}$ and $L_{\lambda,gen,i}$ are the measured and generated values of spectral intensity, respectively. Neglecting the intensity of irradiation from the surroundings which is reflected by the target surface and applying Planck blackbody distribution, Eq. (1), the generated spectral intensity can be simplified as

$$L_{\lambda,gen}(\lambda,T) \cong \varepsilon_\lambda(\lambda) L_{\lambda,b}(\lambda,T) = \varepsilon_\lambda(\lambda)\frac{c_1}{\lambda^5(e^{c_2/\lambda T}-1)}. \tag{14}$$

For emissivity models with exponential form, the linear least-squares technique can be used to determine the inferred temperature and the unknown emissivity coefficients by minimizing the magnitude of χ^2 in the following equation

$$\chi^2 = \sum_{i=0}^{n} (\ln L_{\lambda,meas,i} - \ln L_{\lambda,gen,i})^2. \tag{15}$$

In addition, the Planck blackbody distribution used in Eq. (14) to determinate the generated value of spectral intensity, $L_{\lambda,gen,i,}$ is approximated by Wien's formula,

$$L_{\lambda,b}(\lambda,T) = \frac{c_1}{\lambda^5(e^{c_2/\lambda T}-1} \cong \frac{c_1}{\lambda^5(e^{c_2/\lambda T}-1)}. \tag{16}$$

Therefore, a set of equations that is linear with respect to the temperature and the unknown emissivity coefficients can be created to simplify the computation.

All radiometric methods are sensitive to changes in the spectral emissivity of the material and they also require some knowledge of the surface emissivity. Complex behavior of emissivity variability is the major reason behind the limited accuracy of radiation thermometry. In this study, the interdependent parametric influences of wavelength, temperature, heating time, and alloy composition on steel emissivity were investigated experimentally. Six emissivity models are examined for accuracy in temperature determination subject to the aforementioned parameters.

3. Experimental methods

The experimental apparatus, shown in Fig. 1, was primarily comprised of a spectrometer (radiation thermometer), test sample heating assembly, temperature controller, power supply, translation stage, data acquisition system, and a blackbody for calibration.

A Fast Infrared Array Spectrometer (FIAS) Model ES100 made by Spectraline was optically aligned in front of the test module to perform the radiation intensity measurement. This spectrometer is able to simultaneously measure 160 discrete spectral radiation intensity values over the wavelength range 1.2–4.8 μm. The radiation intensity from the target sample surface is incident on the entrance slit of the FIAS, directed and split into the spectral components, and then ultimately dispersed over a staggered 160 element linear array PbSe detector. The wavelengths and intensities can be found by converting the voltages and pixel numbers recorded on the linear array using pre-installed calibration curves. The intensity data collected in each spectrum is stored at 390 Hz. The entrance slit is 6 mm high by 0.5 mm wide. The FIAS has a 0.5° field of view (FOV) and can accept the incident lights at a divergence angle of ±0.25° from the edges of the slit. Therefore, if the test sample placed at 120 mm in front, the longest side of the homogeneous view area should have at least larger than 7.05 mm ($6 + 2*120*\tan 0.25°$). In addition, a focusing tube may be installed to eliminate the aforementioned spatial resolution problem. Also an alignment HeNe laser can be installed to point the spectrometer at a desired target that is far away from the spectrometer. To record and process the collected data, a computer and two ISA boards were used. The first one is a 1 MHz, 12 bit A/D board, and the second one is a 32 MB memory board. The drive circuit controls the data acquisition in the spectrometer. A Windows-based graphical user interface (GUI) is available for basic spectrometric functions. The output can either be displayed on the Windows-based GUI or stored on the computer for data analysis.

The sample heating assembly which includes cartridge heaters, heating block, test sample, and ceramic fiber blanket insulation, are shown in Fig. 2. The entire sample heating assembly was fastened by the aluminum frame and situated on a two-dimensional trans-

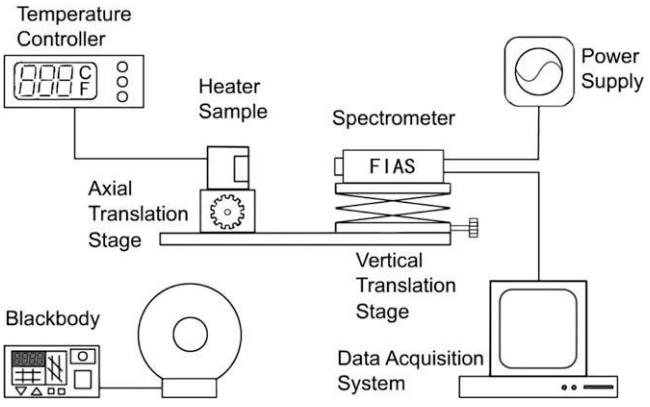

Fig. 1. Temperature measurement facility.

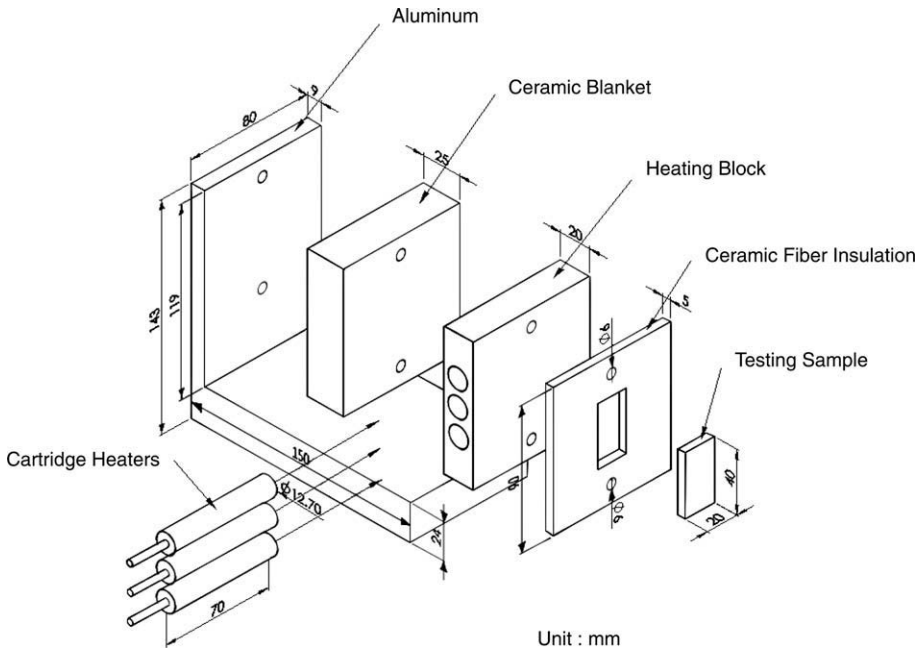

Fig. 2. Construction of steel test sample and heating assembly.

lation stage. The steel test sample was held in contact with a heating block. The heating block having three embedded cartridge heaters whose power was controlled by a temperature controller (WATLOW) with a Chromel–Alumel (type K) thermocouple attached on the sample surface, was used to heat the sample to the desired test temperature. In order to minimize the temperature gradient, the heating block was fabricated from brass and surrounded by a thick blanket of high-temperature ceramic fiber insulation (Thermal Ceramics).

Test samples encompassing a variety of steel were supplied from the Gloria Material Technology Corporation (GMTC), and machined to the size of 40 mm × 20 mm × 5 mm. They are stainless steel (AISI 420 and AISI 630), hot work tool steel (AISI H10 and AISI H13) and cold work tool steel (AISI A2 and AISI A6). Table 1 shows their applications and Table 2 shows the characteristics of each alloy in major constituents as a percentage of weight. The surface profile and average roughness for each sample were measured by a surface profilometer (Alpha-Step MA-1450, Tencor Instrui) and shown in Fig. 3.

Before testing, the test surface was cleaned in succession with acetone and methanol to get rid of oils, grease, and dirt. The tested samples were handled with great care and wrapped in fine tissue. The heating block was preheated to a temperature slightly above the anticipated one before heating the test sample. The test sample was then pressed against the preheated heating block to initiate heat-up. The desired sample temperature was achieved by using the temperature controller to manipulate power input to the cartridge heaters. Once the temperature of the sample was stabilized, the radiance and temperature data were ready to be collected. For this study, three temperatures, 700, 800, and 900 K were selected for measurement and analysis. All of the experiments were operated under normal laboratory conditions with a fairly constant room temperature of approximately 295 K.

The spectrometer was first calibrated by a blackbody, RBB-1000 (MINARAD SYSTEM Inc.), and then aligned with the test sample by the installed HeNe laser. The laser spot aimed at the center of the sample surface. The intensity data from each spectrum was taken by the spectrometer. After the measurements were finished, the heater and spectrometer was powered off. The test sample was then removed from the heating block and allowed to cool down to room temperature.

Table 1
Applications of steel test samples examined in this study.

Type		Applications
Stainless steel	AISI 420	Bolt, palletizer, scalpel, die (plastic)
	AISI 630	Shaft, bolt, valve, family appliance, scalpel, food machine, die (plastic)
Hot work tool steel	AISI H10	Shaft, bolt, die (casting, forging, extrusion),
	AISI H13	Pin, die (casting, extrusion, plastic)
Cold work tool steel	AISI A2	Shaft, accuracy gauge, die (casting, trimming, roller)
	AISI A6	Punch, roller, accuracy gauge, die (casting, trimming)

Table 2
Constituents of steel test samples examined in this study.

Type		Stainless steel		Hot work tool steel		Cold work tool steel	
		AISI 420	AISI 630	AISI H10	AISI H13	AISI A2	AISI A6
Constituents (%)	C	0.33	0.03	0.36	0.39	0.97	0.68
	Si	0.38	0.34	0.91	1.01	0.24	0.28
	Mn	0.38	0.63	0.48	0.33	0.53	2.01
	P	0.022	0.021	0.019	0.021	0.018	0.017
	S	0.004	0.003	0.002	0.001	0.005	0.004
	Ni	0.17	4.60	0.17	0.19	0.14	0.04
	Cr	12.43	15.69	3.24	5.10	4.99	1.02
	Mo	0.06	0.13	2.47	1.25	0.99	0.95
	Cu	0.05	3.31	0.08	0.09	0.05	0.03
	V	0.03	0.08	0.47	0.09	0.18	0.01
	W	0.00	0.03	0.05	0.03	0.08	0.01
	Al	0.028	0.007	0.025	0.026	0.010	0.020
	Co	0.014	0.034	1.895	0.021	0.020	0.006
	N		0.05				
	Ta		0.00				
	Nb		0.28				

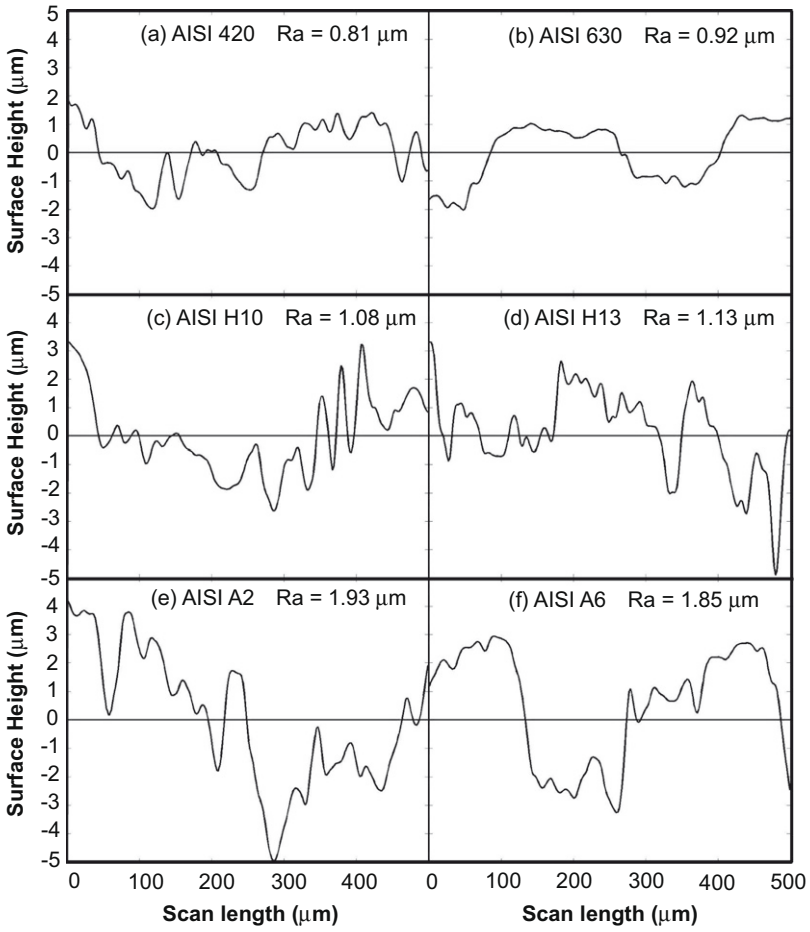

Fig. 3. Surface profiles of steel test samples.

4. Results and discussion

Six different kinds of steel samples divided into three groups were tested in this study. The spectral emissivity was calculated by Eq. (6), where $L_{\lambda,meas}$ was measured by the spectrometer, and $L_{\lambda,b}(\lambda,T)$ and $L_{\lambda,b}(\lambda,T_{sur})$ were calculated from the Planck distribution, Eq. (1), using the sample temperature T from the temperature controller readout, and the room temperature T_{sur}, respectively. Below is a discussion of the effects of temperature, wavelength, heating time, and alloy composition on the spectral emissivity.

4.1. Effects of wavelength

As shown in Table 1, the tested steel samples are divided into three groups for emissivity analysis: stainless steel (AISI 420 and AISI 630), hot work tool steel (AISI H10 and AISI H13) and cold work tool steel (AISI A2 and AISI A6). Spectral distributions of different alloys are similar in the same group. Therefore, one alloy from each group is chosen and shown in Fig. 4 to discuss the spectral effects during the entire examined wavelength range. The results show the emissivity distribution for AISI 630, AISI H10, and AISI A2 at 700 K. The two shaded bands in the figure represent the atmospheric absorption and scattering bands. One centered around 2.7 μm is due to radiation caused by the room humidity and carbon dioxide, and the other one centered around 4.3 μm is due to the room carbon dioxide alone. According to Eqs. (3) and (4), the two bands should be excluded from the examined wavelength ranges since they will affect the intensity measurement and cause errors in calculating the spectral emissivity. As shown in the figure, they separate the emissivity spectrum into three ranges. In shot wavelength range, the distributions for three alloys behave differently. The instability might be due to the higher relative error of the calibration of FIAS in this range [12]. However, in the middle wavelength range 2.91–4.13 μm, all alloys exhibit the expected trend for most metallic surfaces of monotonously decreasing emissivity with increasing wavelength. The same behavior is also observed in the long wavelength range.

4.2. Effects of temperature

Fig. 5 shows the spectral emissivity distribution for AISI 420, AISI H13, and AISI A6 samples at different temperatures, 700, 800 and 900 K from wavelength range 2.91–4.13 μm. The shape of the emissivity spectrum for different alloys keeps linear at different temperatures. However, the spectral emissivity value does not always increase as expected when the temperature increases. The spectral emissivity behaviors for AISI 420 and AISI H13 samples have the expected trend of most metallic surface, increasing emissivity with increasing temperature. The oxidation and the change of surface color from light metallic gray into black during the heating cause the increase in emissivity. However, the emissivity trends for AISI A6, increasing first between 700 and 800 K and then decreasing above 800 K. The decrease in emissivity at high temperature is attributed to the surface color turning from black into red because of the onset of melt, and also the oxide layer volatility [5,13,14].

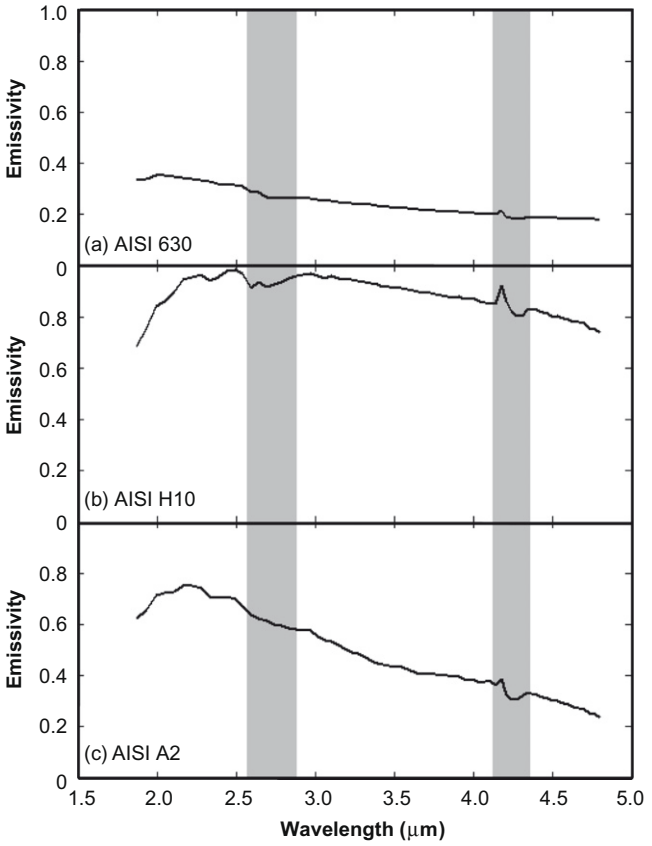

Fig. 4. Effects of wavelength on spectral emissivity for (a) AISI 630, (b) AISI H10, and (c) AISI A2 at 700 K.

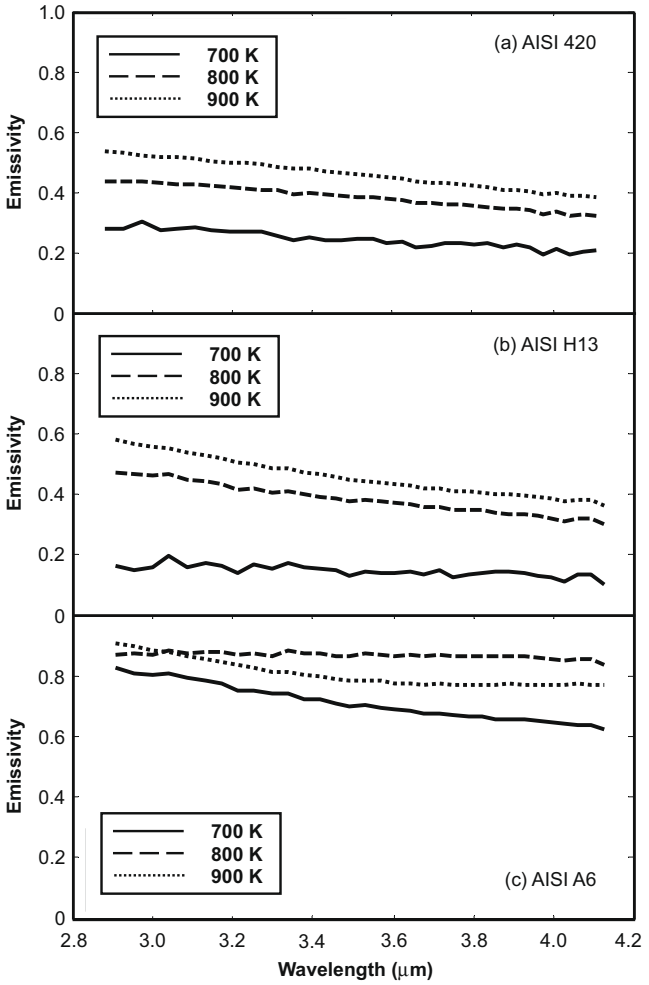

Fig. 5. Effects of temperature on spectral emissivity for (a) AISI 420, (b) AISI H13, and (c) AISI A6.

4.3. Effects of alloy composition

From Fig. 6, we can see the effect of alloying constituents on the spectral emissivity. The spectral emissivity distributions for different alloys are similar in shape, but not in magnitude. The differences in the emissivity are the result of variations in oxidation, which is alloy dependent. AISI 630 has the lowest emissivity over the whole spectral range because it contains high chromium. The surface chromium layer can further prevent the alloy interior from oxidation and confine the growth of oxide layer. Therefore, for steel containing high chromium, emissivity is usually lower than others because of the chromium oxide protection layer.

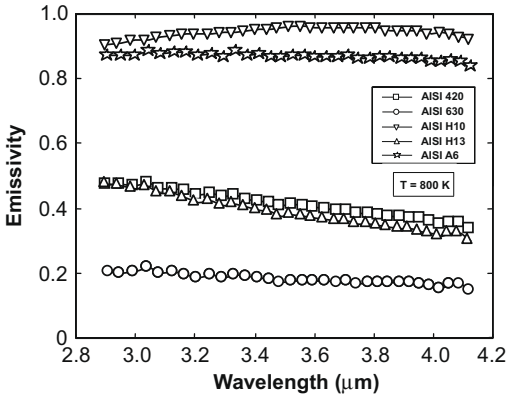

Fig. 6. Effects of alloy composition on spectral emissivity at 800 K.

4.4. Effects of heating time

The effect of the thermal history on spectral emissivity is shown in Fig. 7. Alloys with higher emissivity values have larger change in emissivity during the initial three-hour heating. After the third hour, there is only a slight change in emissivity over the next four hours for most alloys. The surface oxidation is known to contribute to the increase in emissivity value with the time-at-temperature heating. Therefore, following the initial three-hour heating, the oxidation seems to become fully-developed.

5. Application of MRT emissivity models

Six MRT emissivity models discussed earlier, HRR, IST, IST*, IWS, WLT, and WLT* were examined in the present study. Table 3 illustrates the percentage of inferred temperature error predicted by MRT using the six models in the spectral range from 2.91 to 4.13 μm. The CO_2 and H_2O bands shown in Fig. 4 are excluded from the examined wavelength range. In Table 3, it includes results for three groups of steel samples: stainless steel (AISI 420 and AISI 630), hot work tool steel (AISI H10 and AISI H13) and cold work tool steel (AISI A2 and AISI A6), two different number of wavelengths (n and N), and three different temperatures (700, 800, and 900 K). The value n is the required minimum number of wavelength using least-squares technique, which is equal to the number of unknown coefficients in the emissivity model plus two, and N is

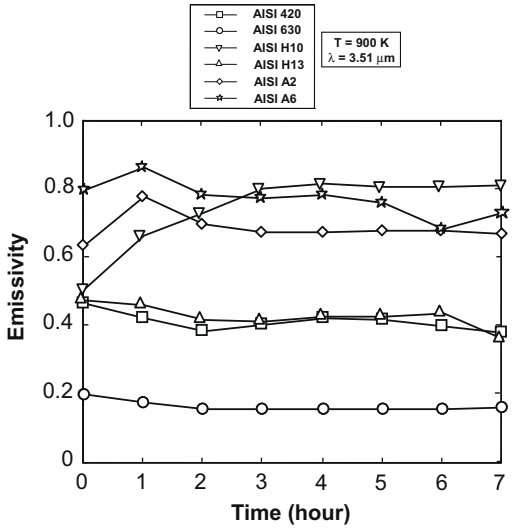

Fig. 7. Effects of heating time on spectral emissivity at 900 K, 3.51 μm.

the total number of wavelength available in the examined wavelength range.

From the results, most of the inferred temperature errors are under 10% and half of them are under 5%. Every model produces its good temperature prediction (under 1%) in certain cases: the HRR model for AISI A2 and AISI A6 at 900 K have temperature errors from 0.2% to 0.4%; the IST model for AISI 630 at 900 K has temperature error 0.9%; the IST* model for AISI H13 at 900 K has temperature error 0.7%; the IWS model for AISI H10 and AISI H13 at 700 and 800 K have temperature errors from 0.1% to 0.7%; the WLT model for AISI 420 at 800 K has temperature error 0.1%, and for AISI A2 and AISI A6 at 800 K have temperature errors from 0.3% to 0.6%; the WLT* model for AISI 630 at 800 and 900 K have temperature errors from 0.2% to 0.7%. Statistically, two emissivity models, WLT and IWS, give most good results and provide the best overall compensation for different alloys, number of wavelengths, and temperatures.

One important feature for MRT is that an increase in the number of wavelengths allows for the statistical reduction in temperature errors from measurement noise. However, as shown in Table 3, increasing the number of wavelengths does not apparently enhance measurement accuracy for most models. The required minimum number of wavelengths, n, actually gives satisfactory results either using linear or nonlinear least-squares technique in this study. This observation is consistent with the findings by Doloresco [11], Gathers [15], and Gardner [16]. Therefore, it is sufficient to employ the required minimum number of wavelengths to infer the temperature.

The percentage of inferred temperature error predicted by the best model for each alloy at different temperatures and number of wavelengths are shown in Table 4. Statistics show that the IWS model occupies the most and the WLT model comes in second. This similar result was also found earlier in Table 3. This coincidence shows that the emissivity models, WLT and IWS, not only achieve good temperature predictions for different alloys, number of wavelengths, and temperatures, but also provide the smallest inferred temperature errors. The other models have their best result in some conditions: the WLT* model for AISI 630 at 800 and 900 K, and the HRR model for AISI A2 and AISI A6 at 900 K. Overall the IST model shows the poorest compensation and is not recommended for steel samples in MRT.

How an emissivity model to affect the accuracy of temperature prediction is demonstrated here through the following example. As shown in Table 3, for AISI A6 at 800 K with number of wavelengths *N*, three representative emissivity models, IST, IWS and WLT have temperature errors, 1.5% (812.0 K), 0.8% (793.2 K) and 0.3% (798.0 K), respectively. In other words, in this case the WLT model is the most accurate MRT emissivity model in temperature determination, followed by the IWS model, and then the IST model. Fig. 8(a) shows the comparison of the measured spectral intensity for AISI A6 at 800 K and the generated spectral intensity in Eq. (14) which is inferred by the emissivity models, IST, IWS and WLT. There is no much difference among them since the least-squares technique in Eq. (13) is applied. The generated spectral intensity value, $L_{\lambda,gen,i,}$ from each emissivity model should be in between the measured spectral intensity value, $L_{\lambda,meas,i}$ in order to minimize the chi-squared (χ^2) value and determine the inferred temperature

Table 3
Percentage of temperature error in inferred temperature by MRT for steel samples at 700, 800 and 900 K.

Inferred temperature errors (%), from 2.91 to 4.13 μm															
Sample		*T* (K)	Model	HRR		IST		IST*		IWS		WLT		WLT*	
			Wave. No.#	*n*	*N*	*n*	*N*	*n*	*N*	*n*	*N*	*n*	*N*	*n*	*N*
Stainless steel	AISI 420	700		7.2	8.0	11.2	8.8	14.0	12.2	0.6	3.0	3.9	2.3	5.9	7.9
		800		9.8	9.5	10.7	10.5	1.1	8.4	2.0	2.3	1.1	0.1	11.3	9.9
		900		14.1	12.5	12.9	13.0	9.8	11.3	1.1	0.9	1.4	1.9	11.0	11.4
	AISI 630	700		5.1	5.1	4.9	4.7	10.8	1.2	7.3	7.5	4.3	5.2	5.7	4.5
		800		9.6	5.7	3.6	2.1	2.2	14.2	8.3	9.8	9.0	8.2	0.6	1.7
		900		6.5	4.8	1.7	0.9	7.1	8.0	10.7	11.5	9.7	9.3	0.2	0.7
Hot work tool steel	AISI H10	700		1.4	1.6	5.7	6.0	1.3	1.1	1.8	0.1	2.2	2.6	5.4	6.1
		800		9.1	10.0	2.0	2.8	1.4	1.2	0.2	0.4	1.6	1.7	2.2	2.7
		900		11.3	8.5	14.1	12.0	19.2	19.8	0.8	0.9	3.9	2.1	12.5	10.3
	AISI H13	700		8.1	7.0	5.1	2.3	32.6	19.0	4.4	7.5	10.2	8.3	1.2	1.1
		800		17.8	18.2	14.6	14.6	16.6	6.8	0.7	0.5	2.7	3.2	13.8	14.5
		900		23.3	21.7	18.4	17.9	7.7	0.7	3.4	2.8	5.8	6.1	17.0	17.5
Cold work tool steel	AISI A2	700		19.8	18.2	13.3	16.6	7.6	4.5	3.2	2.9	2.9	5.0	12.7	15.8
		800		0.9	3.4	6.4	4.6	2.7	3.5	1.5	0.5	0.5	0.6	3.9	3.9
		900		0.2	0.3	8.5	9.0	2.8	2.8	0.8	1.4	2.6	3.3	7.3	8.3
	AISI A6	700		5.3	1.9	6.4	11.5	3.2	3.2	3.6	5.6	1.2	3.1	3.8	6.1
		800		6.8	6.9	1.2	1.5	1.9	1.8	0.9	0.8	0.3	0.3	1.7	1.5
		900		0.2	0.4	8.7	9.3	11.4	8.2	1.1	1.2	4.0	3.5	9.6	8.8

Wave. No. represents the number of wavelength: *n* is minimum number of wavelength required in MRT model and *N* is total number of wavelength available in the examined wavelength range.

Table 4
The best model and the percentage of temperature error for each steel sample.

Sample		Minimum temperature error (%)					
		700 K		800 K		900 K	
		$n^{\#}$	N^{*}	n	N	n	N
Stainless steel	AISI 420	0.6 (IWS)	2.3 (WLT)	1.1 (WLT)	0.1 (WLT)	1.1 (IWS)	0.9 (IWS)
	AISI 630	4.3 (WLT)	1.2 (IST*)	0.6 (WLT*)	1.7 (WLT*)	0.2 (WLT*)	0.7 (WLT*)
Hot work tool steel	AISI H10	1.3 (IST*)	0.1 (IWS)	0.2 (IWS)	0.4 (IWS)	0.8 (IWS)	0.9 (IWS)
	AISI H13	1.2 (WLT*)	1.1 (WLT*)	0.7 (IWS)	0.5 (IWS)	3.4 (IWS)	0.7 (IST*)
Cold work tool steel	AISI A2	2.9 (WLT)	2.9 (IWS)	0.5 (WLT)	0.5 (IWS)	0.2 (HRR)	0.3 (HRR)
	AISI A6	1.2 (WLT)	1.9 (HRR)	0.26 (WLT)	0.25 (WLT)	0.2 (HRR)	0.4 (HRR)

[#] n is minimum number of wavelength required in MRT model.
[*] N is total number of wavelength available in the examined wavelength range.

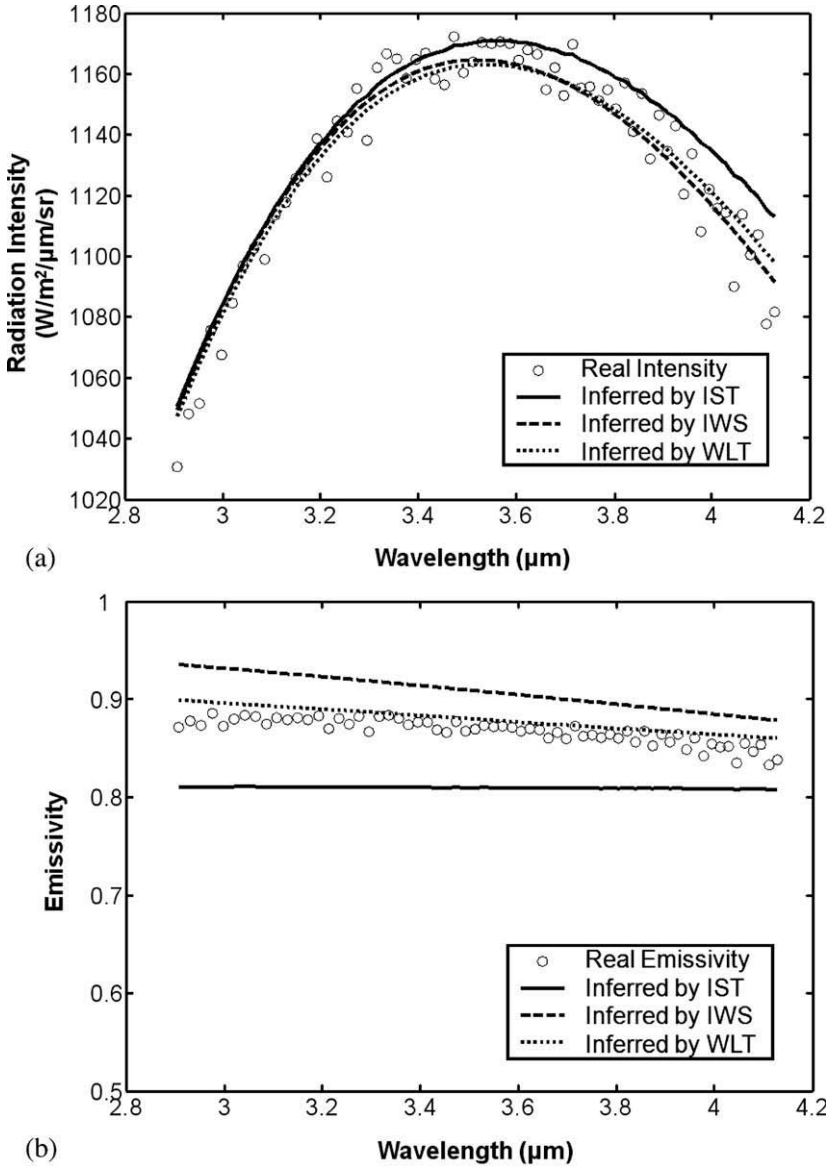

Fig. 8. Comparison between experimental data and predictions of IST, IWS, and WLT model for (a) radiation intensity and (b) spectral emissivity of AISI A6 at 800 K.

and the unknown emissivity coefficients. However, in Fig. 8(b), there is a big difference between the real emissivity value and that inferred from each model. The emissivity distribution inferred by the WLT model which has the most accurate temperature prediction is the closest one to the real emissivity distribution. The next closer to the real emissivity spectrum is the one inferred by the IWS model which has the second best temperature prediction. The furthest one away from the real emissivity values is inferred by the IST model which has the worst temperature prediction. Therefore, we can find that the closer the generated emissivity

spectrum and the measured one, the more accurate inferred temperature, i.e. if the emissivity model can well represent the real emissivity behaviors, the more accurate inferred temperature can be achieved.

6. Conclusions

In this study, experiments were performed to measure the emissivity values for various steel samples. The effects of different parameters on spectral emissivity, such as wavelength, temperature, alloy composition, and heating time are investigated. The experimental work is complemented by six emissivity models to examine Multispectral Radiation Thermometry (MRT) on inferring surface temperature. Key findings from this study are discussed below.

For steel emissivity behaviors, all steel alloys overall exhibit the expected trend for most metallic surfaces of monotonously decreasing emissivity with increasing wavelength. However, the spectral emissivity value does not always increase as expected when the temperature increases. Due to surface oxidation and discoloration, the change of the surface color from light metallic gray into black causes the increase in emissivity between 700 and 800 K. However, the decrease in emissivity between 800 and 900 K is attributed to the surface color turning from black into red because of the onset of melt, and also the oxide layer volatility. The spectral emissivity distributions for different alloys are similar in shape, but not in magnitude. For steel containing high chromium, emissivity is usually lower than others because of the chromium oxide protection layer. The emissivity value becomes fairly constant following the initial three-hour heating, which points to the surface oxidation becoming fully-developed.

For the assessment of MRT emissivity models on steel samples, most emissivity models provide the percent error of inferred temperature under 10% and half of the results are under 5%. Every model also produces its good temperature prediction (under 1%) in certain conditions. Two emissivity models, WLT and IWS, give most good results and provide the best overall compensation for different alloys, number of wavelengths, and temperatures. Increasing the number of wavelengths does not significantly improve measurement accuracy for most models. It is sufficient to employ the required minimum number of wavelengths to infer the temperature while using MRT least-squares technique. The results based on MRT least-squares technique reveal that the closer the generated emissivity spectrum and the measured one, the more accurate inferred temperature. Therefore, if the emissivity model can well represent the real emissivity behaviors, the more accurate inferred temperature can be achieved.

Acknowledgments

The author is grateful for the support of the National Science Council of Taiwan (with project number NSC-94-2218-E-006-046). The author would also like to thank the Gloria Material Technology Corporation (GMTC) in Taiwan for the supply of steel samples and Dr. Jongmook Lim of the Spectraline Inc. for the technical assistance and the instrument support.

References

[1] V.D. Dmitriev, G.K. Kholopov, Radiant emissivity of tungsten in the infrared region of the spectrum, Zh. Prikladnoi Spektroskopii 2 (6) (1965) 481–488.
[2] M.J. Haugh, Radiation thermometry in the aluminum industry, in: D.P. DeWitt, G.D. Nutter (Eds.), Theory and Practice of Radiation Thermometry, John Wiley and Sons, New York, 1988, pp. 905–971.
[3] F.A. Mihalow, Radiation thermometry in the steel industry, in: D.P. DeWitt, G.D. Nutter (Eds.), Theory and Practice of Radiation Thermometry, John Wiley and Sons, New York, 1988, pp. 861–904.
[4] M.A. Pellerin, Multispectral Radiation Thermometry: Emissivity Compensation Algorithm, M.S. Thesis, Purdue University, West Lafayette, IN, 1990.
[5] M.A. Pellerin, Multispectral Radiation Thermometry for Industrial Application, PhD Thesis, Purdue University, West Lafayette, IN, 1999.
[6] C. Wen, I. Mudawar, Emissivity characteristics of roughened aluminum alloy surfaces and assessment of multispectral radiation thermometry (MRT) emissivity models, Int. Commun. Heat Mass Transfer. 47 (2005) 3591–3605.
[7] C. Wen, Emissivity Characteristics of Aluminum Alloy Surfaces and Assessment of Multispectral Radiation Thermometry (MRT) Emissivity Models, PhD Thesis, Purdue University, West Lafayette, IN, 2005.
[8] T. Duvaut, D. Georgeault, J.L. Beaudoin, Multiwavelength infrared pyrometer: optimization and computer simulations, Infrared Phys. Technol. 36 (1995) 1089–1103.
[9] G.J. Dail, M.G. Fuhrman, D.P. DeWitt, Evaluation and extension of the spectral-ratio radiation thermometry method, in: Proceedings 4th Int. Aluminum Extrusion Technology Seminar, vol. 2, Chicago, IL, 1988, pp. 209–213.
[10] P.B. Coates, Multi-wavelength pyrometry, Metrologia 17 (1981) 103–109.
[11] B.K. Doloresco, Review of Multispectral Radiation Thermometry and Development of Constrained Minimization Method, M.S. Thesis, Purdue University, West Lafayette, IN, 1986.
[12] J. Ji, J.P. Gore, Y.R. Sivathanu, J. Lim, Fast infrared array spectrometer used for radiation measurements of lean premixed flames, in: Proceedings of NHTC'00, 34th National Heat Transfer Conference, Pittsburgh, PA, 2000, pp. 1–6.
[13] A. Otsuka, K. Hosono, R. Tanaka, K. Kitagawa, N. Arai, A survey of hemispherical total emissivity of the refractory metals in practical use, Energy 30 (2005) 535–543.
[14] G.R. Smolik, K.A. McCarthy, W.J. Garmack, K. Coate, Mobilization from austenitic stainless steel in air and steam: recent test, compilation of data from tests to data, and resulting dose calculations, fusion engineering, in: 17th IEEE/NPSS Symposium, vol. 1, 1997, pp. 161–166.
[15] G.R. Gathers, Analysis of multiwavelength pyrometry using nonlinear Chi-square fits and Monte Carlo methods, Int. J. Thermophys. 13 (3) (1992) 539–554.
[16] J.L. Gardner, T.P. Jones, M.R. Davies, A six-wavelength radiation pyrometer, High Temp.: High Press. 13 (1981) 459–466.